

Strengthening the Self Compacting Reinforced Concrete Dapped Ends with Near Surface Mounted (NSM) Steel Bar Technique

Qasim M. Shakir^{a,*}, Ruqyia Alliwe^a

^aFaculty of Engineering, University of Kufa, Al-Najaf, Iraq

Corresponding author: *qasimm.alabbasi@uokufa.edu.iq

Abstract—An experimental study has been conducted to explore the response of reinforced self-compacting concrete dapped ends retrofitted with NSM steel bars. Eleven specimens are tested with two shear slenderness ratio values (a/d), namely (1.0 and 1.5). Deficiencies in reinforcement in the nib and hanger zone are considered. The response is studied in terms of loading history, cracking and failure load, failure mode, cracking pattern, toughness, stiffness, and ductility. It is observed that retrofitting the nib region with horizontal bars improved the capacity by 29% and 20% for the two shears span/depth (a/d) values, respectively. The maximum enhancement in the capacity for upgraded hanger regions with $a/d = 1$ is about 21%. Regarding toughness, this research indicated that for reduced nib steel specimens with $a/d=1.0$ and 1.5, a reduction by 17% and 27%, respectively, were obtained. Whereas reducing the hanger steel by 30% led to a drop by 29%. Strengthening of deficient nib reinforced specimens with $a/d = 1.0$ and 1.5 led to an improvement in toughness by 43% and 62%, respectively. For specimens with deficient hanger steel ($a/d=1.0$), the strengthening led to toughness enhancement by 87%. Strengthening of deficiently reinforced nib end with the two a/d values resulted in improving stiffness by 18% and 24%, whereas when strengthening the hanger zone, an enhancement of 9% is obtained. For ductility, it is concluded that the prediction of ductility ratio using the displacement ratio method is more efficient than the toughness ratio method because it is considered the premature failure cases. Also, it is obtained that increasing the a/d value resulted in reducing the ductility ratio.

Keywords— High strength; self-compacting; NSM steel bar; strengthening; dapped end beam; fictitious hinge.

Manuscript received 2 Feb. 2019; revised 12 Oct. 2020; accepted 10 Dec. 2020. Date of publication 30 Apr. 2021.
IJASEIT is licensed under a Creative Commons Attribution-Share Alike 4.0 International License.



I. INTRODUCTION

The dapped end beams are a precast reinforced concrete package with less depth at the end of the beam. However, the flow of internal forces is interrupted by a sudden change in geometry. Then, disturbed regions are created around the re-entrant corner and in the nib. Two methods were suggested to treat such regions: the shear friction method (PCI) [1] and the STM model. Such zones may be subjected to high stresses as well as to unforeseen forces such as horizontal forces due to temperature changes. Besides, dapped end allows getting a better fabrication with columns in connection. They are also used to reduce the structure's overall height and increase stability to support the bearing. They are usually used in reinforced concrete structures such as prefabricated buildings, parking structures, and recently prefabricated conveyors belts, the bridge girder, precast footings [2].

Many researchers studied the behavior and strengthening of reinforced concrete DEB. Mattock and Chan [3] reported that the use of the corbel design concepts in the dapped end is

valid for ($a/d < 1$) but with adding hanger reinforcement. Liem [4] showed that the ultimate strength of dapped end with (45°) inclined reinforcement two times the strength of the case with horizontal or vertical reinforcement". Lu *et al.* [5] studied several variables that may influence on the behavior, such as the concrete strength, (a/d) value, and amount of main reinforcement. Ahmad *et al.* [6] reported that the design for DEB using STM model is dependent on the angle of strut inclination. Aswin *et al.* [7] studied several variables as numbers of the nib reinforcement, main flexural reinforcement, and concrete type at the dapped end region. Results indicated that the use of fibrous reinforced concrete in the dapped area improved the failure load by (51.9%). While increasing the number of the nib and main flexural reinforcements enhanced the failure load by (62.2%) and (46.7%) respectively.

Regarding the strengthening of the dapped end beams; Tan investigated several configurations to strengthen dapped end beams in shear. Carbon FRP plates (CP) and sheets (CS) in addition to glass fiber fabrics (GS). Results indicated an increase in the ultimate load of 43, 75 and 80 percent for the

CP, CS and GS systems, respectively. With using suitable anchorage bolt in the strengthening systems, further enhanced occurred in the strength of 16 %, 33% and 41% for the CP, CS and GS systems, respectively. Huang and Myers (2006) used the FRP composites on strengthening precast prestressed concrete double tee members. Two strengthening arrangements have been considered. A 0°/90° wrapping technique was used. It was deduced that the application of the U-anchor system to the externally bonded FRP laminates increased the ultimate capacity of a dapped-end and ensured fiber rupture instead of deboning of the FRP sheets. Afefy *et al.* [10] conducted experimental and analytical study to investigate the efficiency of external bonding (EB) technique using CFRP strips and sheets to retire the full capacity of deficiently reinforced stepped beams.

It was concluded that the proposed schemes might restore the total capacity of the mid detailed beam with excess in capacity compared to the detailed stepped beam by about 15%. Sas *et al.* [11], proposed nonlinear FEA modeling to study the most suitable scheme of (CFRP) composites to strengthen RC DEBs. 24 external bonding and NSM (Near Surface Mounted) reinforcement configurations have been considered. Several parameters were considered, including CFRP characteristics, the strengthening arrangement, and the angle of the sheets' inclination. Rupture and debonding failure modes of the CFRP were observed. It was drawn out that high strength NSM FRPs might enhance the capacity of DEBs. Taher [12] studied the strengthening of DEB with different techniques such as bonding of steel angle at the recessed corner, unbounded inclined steel bolt anchoring in pre-drilled hole, external steel plate jacketing, exterior carbon fiber wrapping within the beam stem, exterior CFRP stripping, and combination of carbon fiber wrapping and strapping. It was concluded that the mode of failure was influenced by the introduced reinforcement detailing defect in the recess zone. Atta and Taman [2] considered strengthening reinforced concrete DEB with different shapes of external prestressing technique directions, such as horizontal, vertical, and inclined. They concluded that the vertical external prestressing technique is an effective strengthening method to increase the capacity of DEB up to 82%.

Shakir and Abd [13] studied the response of reinforced self-compacting concrete dapped end beams strengthened by CFRP sheets. It is found that a deficiency in nib reinforcement by (60%) decreased the capacity by (36%) and (15%) for $a/d=1.5$ and $a/d=1.0$, respectively. Furthermore, enhancements in the capacity of (17% and 23%) for the two a/d values respectively when using inclined strips in upgrading the hanger region, whereas the enhancements were (11% and 18%) for a/d (1.5 and 1.0) respectively when using vertical stripes. For specimens with $(a/d) = 1.5$ and strengthened at nib region, the enhancement was (10%).

Many studies used the NSM technique in strengthening RC beams using CFRP rods [14]–[16], CFRP laminates and strips [17], [18], Aluminum alloy bars [19], and steel bars [20]. Compared to external bonding strengthening technique, the NSM system has merits, including:

- As the concrete cover protects them, there will be less exposure to external effects as fire, environmental and accidental effects, which is essential for strengthening negative moment regions.

- The amount of surface preparation in the site may be reduced; only grooving is required.
- NSM bars may be easily installed into members to avoid failure modes of the debonding type. Thus, NSM reinforcement is less prone to debonding from the externally bonded strengthening sheets.
- The aesthetic of the strengthened structure is virtually unchanged.

Few studies used the NSM steel bar technique in strengthening the Disturbed regions as corbels and dapped ends. Shakir and Kamonna [13] conducted an experimental investigation to study the adequacy of NSM steel bar strengthening technique to improve the performance of deficiently reinforced high strength self-compacting concrete corbels strengthened with NSM steel bars. The work includes testing ten specimens that are grouped into two categories with two values of shear span/depth ratio (a/d). It was reported that retrofitting RC corbel with NSM steel bar technique enhanced the load capacity noticeably by 57% and 41% for a/d of 0.85 and 1.25, respectively. The upgrading configuration termed as "Upside down V-shaped" is adequate for ($a/d < 1$). The horizontal bars configuration is more effective for large a/d values ($a/d > 1$). There is no previous study considered using the NSM steel bars technique to strengthen the dapped ends. But due to the reliable results obtained by Shakir and Kamonna [13] on RC corbels; this application is extending in the present work to concern the dapped end beams.

II. MATERIAL AND METHOD

In the present work, an experimental study was carried out to investigate the behavior of self-compacting reinforced concrete dapped ends strengthened by NSM steel bar technique. Two values of shear slenderness ratios have been considered to study this parameter's effect on the response of dapped ends and the impact of the case when a bending moment or shear force is dominant. Also, the efficiency of strengthening of deficiently reinforced specimens at nib and hanger zones is investigated. It is to be mentioned that the specimens with reduced hanger steel are considered only with $a/d=1.0$. Because that with $a/d=1.5$, the weak region is shifted to be within the nib end. Thus, it is expected that failure occurs within the nib end and is not controlled by hanger steel behavior.

A. Materials Properties

The proportions of the constituent materials of the self-compacting concrete mix used in the present work are listed in Table 1. Such components are cement, water, coarse aggregate (gravel), fine aggregate (sand), limestone powder, superplasticizer, steel bars, and epoxy. All tests except those of steel are achieved at the Structural Laboratory in the Department of Civil Engineering / Faculty of Engineering / Kufa University. Steel tests are performed at the structural laboratory/ Bureau consultant of the University of Kufa. Three bar sizes are used, $\Phi 10$, $\Phi 12$, and $\Phi 16$, with yield stresses of 568 MPa, 615 MPa, and 634 MPa, respectively, and ultimate strengths of 726 MPa, 712 MPa, and 748 MPa, respectively.

TABLE I
CONSTITUENT MATERIAL OF THE CONCRETE MIX

Constituents' materials	Quantity/m3
Cement (kg)	400
Fine Aggregate (kg)	962
Course Aggregate (kg)	780
Limestone Powder (kg)	75
Water (kg)	128.7
Water/ Cement Ratio	0.32
Superplasticizer (L)	4.8

B. Description of Specimens

For all specimens, the cross-section dimensions where the overall length was (1600mm) (200mm) width, (400mm) height, and. The nibs had a size of (250mm) and an overall depth of (200mm). The program consists of testing 12 samples under static load. They are grouped into two sets. Group A in which all specimens are tested under $a/d=1.0$. It consists of eight specimens, one control (reinforcement 100%), one with 50% nib reduced steel, two are strengthened at nib zone, one with 30% reduced hanger steel and three are reinforced at the hanger zone three different angles.

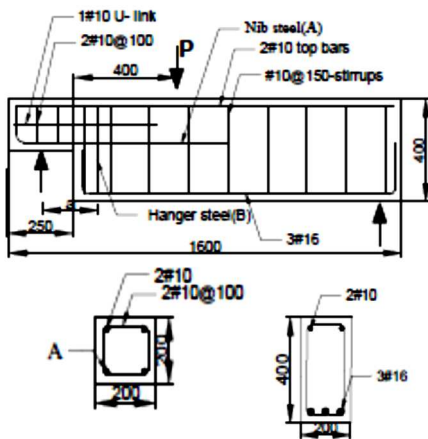


Fig. 1 Details of reinforcement for typical specimens

The second group in which all specimens are tested under a/d value of 1.5 consisted of one control specimen (full reinforcement), one with 50% reduced nib steel and two are strengthened at nib zone using the same schemes in the corresponding samples with $a/d=1.0$ Fig. 1 shows the reinforcement detailing and dimensions of the tested specimens. Furthermore, Table 2 shows the number of bars at nib and hanger for the control, reduced nib steel and reduced hanger steel specimens.

TABLE II
REINFORCEMENT QUANTITIES FOR THE TESTED HALF JOINTS

Control specimens	Specimens with Reduced	
	hanger steel	Nib steel
Nib steel(A)	2#16	2#12
Hanger steel(B)	3#10	3#10

C. Strengthening by NSM steel bars

In the research program, the strengthening of specimens is selected carefully based on the pattern of the cracks of control beams. Table 3 shows the detailing of the strengthening of the tested beams. Several configurations are investigated for both nib and hanger regions, as shown in Fig. 2.

TABLE III
CHARACTERISTICS OF BEAMS TESTED AND PARAMETERS INVESTIGATED

Group	Symbols	Strengthening Method
G1($a/d=1.0$)	C001	Full reinforcement
	RN01	50% reduced nib reinforcement
	SNH1	Strengthened with one horizontal steel bar in each face $\varnothing 12$.
	SNI1	Strengthened horizontal bar + inclined steel bar with angle 45° in each face $\varnothing 10$.
	RH01	30% reduced hanger reinforcement
	SHV1	Strengthened with two vertical steel bar $\varnothing 10$ with angle 90° in each face.
	SHF1	Strengthened with two inclined steel bar $\varnothing 10$ with angle 45° in each face.
	SHT1	Strengthened with two inclined steel bar $\varnothing 10$ with angle 30° in each face.
G2($a/d=1.5$)	C002	Full reinforcement
	RN02	50% reduced nib reinforcement
	SNH2	Strengthened with one horizontal steel bar in each face $\varnothing 12$.
	SNI2	Strengthened horizontal bar + inclined steel bar with angle 45° in each face $\varnothing 10$.

D. Test Setup

Each specimen is tested in a universal testing machine at the University of Kufa at the capacity of 2000 kN. The tested dapped end beams are simply supported with span of 1600 mm, 400 mm depth and 200 mm width with a/d ratios of 1.0 and 1.5. The steel bearing plate has dimensions 100 mm x 200 mm x 10mm. The dapped end beams are loaded with one-point load and tested under static loading as showing in Fig. 3.

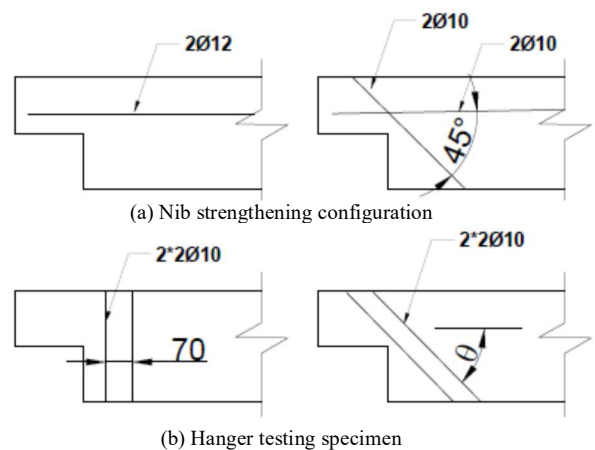


Fig. 2 Strengthening schemes used in the present work.



(a) Universal testing machine



(b) Recording deflections with LVDT

Fig. 3 Testing machine and displacement records

III. RESULTS AND DISCUSSION

The results of the experimental tests of all reinforced concrete dapped end beams were tested. As the first crack, failure load, and the modes of failure are listed in Table 2. In all control beams, the first cracks initiated at the re-entrant corner of the dapped end. While in strengthened beams, the first crack occurred at the mid-span of the beam that developed diagonally or vertically towards the point load.

TABLE IV
RESULTS OF THE TEST DAPPED END BEAMS

Group	Symbols	Δu_1	Pcr	Δu_2	Pu
G1(a/d=1.0)	C001	8.85	65	8.6	371
	RN01	9.24	60	8.1	330
	SNH1	9.44	75	9.1	425
	SNII	9.09	75	7.95	355
	RH01	8.90	70	7.85	350
	SHV1	10.8	75	9.6	425
	SHF1	11.88	70	9.15	400
G2(a/d=1.5)	SHT1	7.1	65	7	335
	C002	11.6	60	8.2	250
	RN02	12.15	65	7.5	238
	SNH2	7.79	50	7.15	285
	SNI2	9.91	70	8.4	295

Δu_1 : Deflection at nib end; Δu_2 : Deflection under load; Pcr: Cracking load; Pu: Failure load

In all control beams, the first cracks initiated at the corner of dapped end beam, while in strengthened beams, the flexural shear crack was the first crack occurred at the mid-span of the beam with the vertical or diagonal trend the point load. The cracking load, ultimate load, and deflection at ultimate stages are listed in Table 4. The discussions of results obtained for the specimen are presented in the following sections.

A. Control Specimens (C001, C002):

The load-deflection curves for the control specimens' results are depicted in Fig. 4. It can be concluded that reducing (a/d) value from 1.5 to 1.0 results in increasing the failure load capacity by about (32.6%). The map of cracking propagation at failure for specimen C001 is depicted in Fig. 5. The first crack occurred with a load of 65 kN at the re-entrant corner, which represents the most critical location of the half joint with an angle of about 47°. This result agrees with Wang et al. [22] that this angle lies in (40-60) o. This variation depends on the ratio of bending moment/shear force applied on the half-joint, detailing nib and hanger reinforcement and concrete properties. Due to the U-stirrups' existence within the nib end, more cracks developed parallel to the first crack. A fictitious hinge is developed at the level when the first diagonal crack changes its inclination to be horizontal affected compressive stresses, as shown in Fig. 6. This hinge formation resulted in rigid body rotation of the dapped end and the beam relative to the hinge. The free-body diagram for both parts is affected by the two ties; one is represented by tension in the main nib steel and vertical, which represents the tension of the hanger reinforcement.

Regarding the full depth beam, it seems to behave as simply supported at the fictitious hinge. Thus, the efficiency of the bond of the main tensile steel at the bottom corner (CTT) nodal point, as shown in Fig. 6 acts as the controlling parameter in determining the range of resistance. Due to the high resistance of the anchorage steel, cracks initiated away from the nodal point. Further load resulted in more curvature of the beam and cracks shifted towards the zone of maximum bending moment.

Failure of the dapped end is controlled by the deterioration in the compression strut of concrete or failure of the bond at the nodal point (CTT) of the beam's main steel. It is observed that the failure occurred due to the first case. i.e., as a "diagonal shear at the re-entrant corner". As the ratio of (bending moment/shear force) increased, be adopting higher a/d value as in specimen C002. The tensile tie (horizontal nib reinforcement) is subjected to more stresses. Thus, more deflection can be recorded with the same load, and some cracks initiated at the nodal point (CTT).

Moreover, the extended end behaves as to be hinged at the fictitious hinge. Hence, more curvature can be seen. Consequently, the horizontal cracking extends to the tip end of the nib. Compared to the case in specimen C001, the shear may be dominant, and the development of the horizontal crack is restricted. It is to be mentioned that the first crack also, initiated at the re-entrant corner with a load of 60 kN. However, with a smaller angle of inclination of 45°, the specimen C002 failed by shear at the extended end with some crushing at the compression face.

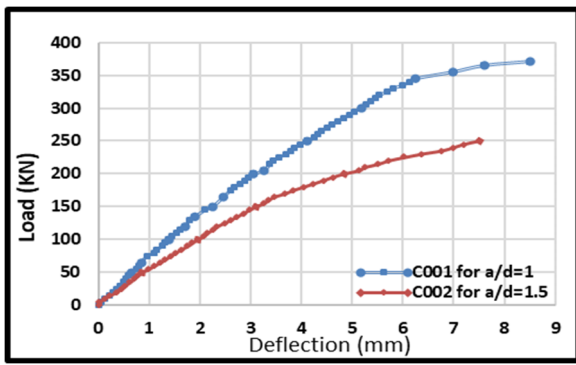
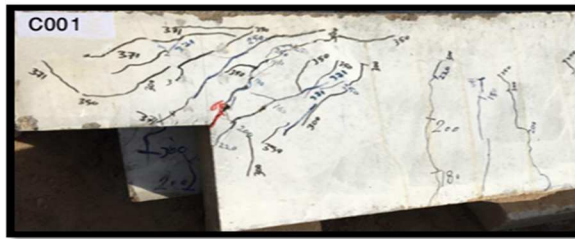
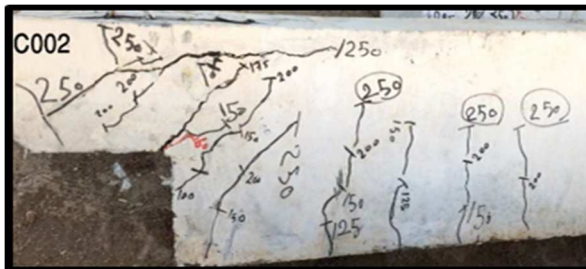


Fig. 4 Load-deflection curves for specimens with different (a/d) ratio



(a) Specimen C001



(b) Specimen C002

Fig. 5 Cracks patterns at failure for the Control Specimen

It is expected that more capacity can be obtained when the compressive force is improved by using a higher grade of concrete within the dapped end region.

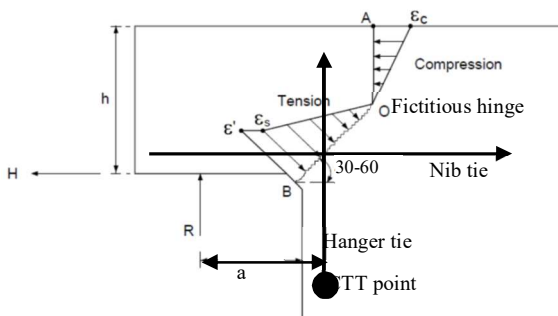


Fig. 6 Fictitious hinge within a dapped end.

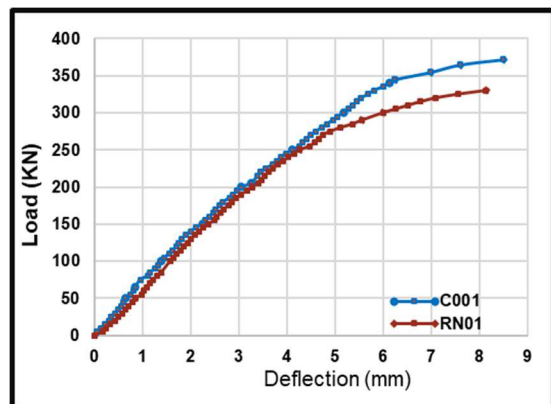
B. Specimens Control Reduced Reinforcement (RN01 & RN02)

Loading history curves for the two specimens are represented compared to the reference specimen are shown in Fig. 7. The reduction in nib reinforcement decreases the failure load and deflection by about 11% and 6%, respectively, for specimen RN01. Besides, it is recognized that the specimen RN02 has a small effect of reducing the nib reinforcement of the dapped end with (a/d=1.0), where a reduction in the failure load and deflection about 5% both.

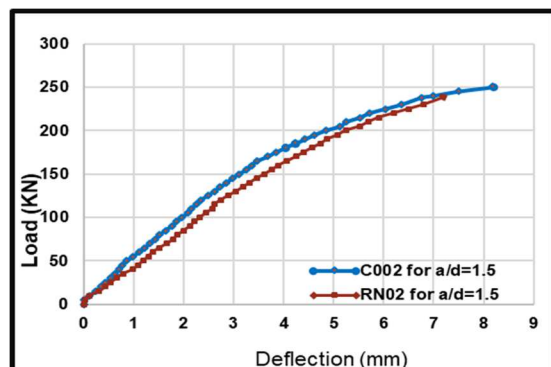
The minor differences between the control specimens (with full nib reinforcement) and the specimens of reduced steel may be attributed to the fact that the PCI method overestimates the steel amounts with self-compacting high strength concrete, a need to introduce some modifications on the method to consider this topic.

Fig. 8a shows the history of crack propagation for the deficient nib reinforced specimen with a/d=1.0, specimen RN01. Compared to the control specimen C001, more cracks developed near the nodal point (CTT) at bottom corner of the depth beam due to more flexible behavior of the beam portion that acquired. More rotation about the fictitious hinge due to the lack in nib steel has occurred. The first crack initiated diagonally at the re-entrant corner as in the specimen C001. The smaller angle of inclination of the cracks has been measured of less 45°. At the loading stage of 125kN, cracking at the compression face initiated. This crack may be interrupted by the cracks developed from the support, causing more weakening in the nib steel bond.

For the specimen RN02, Fig.8b, the cracking initiated firstly at the re-entrant corner with an angle of about 30° and that the fictitious hinge developed closer to the point of load application with a lower level than the specimen RN01 (1/2 nib depth). Consequently, the nib end portion behaves more flexibly and the horizontal crack in the top fibers does not extend as in specimen RN01, C001 or C002, because that the cracking initiated to form the support soon becomes the critical solution. For the beam portion, it can be observed that most cracks are concentrated close to the nodal point (CTT) with a smaller load. Both specimens failed by diagonal shear failure in the nib end.

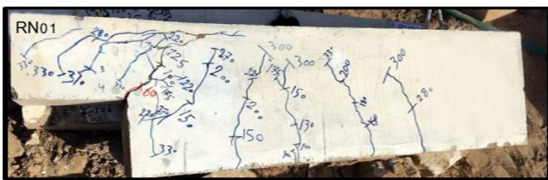


a) Specimen RN01 against C001

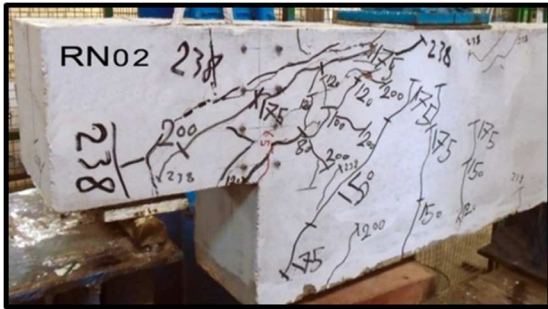


b) Specimen RN02 against C002

Fig. 7 Load deflection curves for the specimens RN01 and RN02 against the control specimens



(a) Specimen RN01



(b) Specimen RN02

Fig. 8 Cracks patterns for the specimens with reduced reinforcement at nib region

C. Specimens SNH1 & SN11; (a/d) = 1.0

The first strengthening scheme adopted to restore the capacity of the specimen RN01 is the horizontal configuration SNH1. It can be seen from Fig. 9 that the maximum enhancement in load capacity is due to the horizontal configuration, and it is about 29% to specimen (RN01), i.e., and 15% over the capacity of the specimen (C001).

The crack pattern for specimen SNH1, Fig. 10a reveals that the first crack initiated at the re-entrant corner within a load level of 75 kN. However, the horizontal cracking propagation at the top fibers is interrupted by the vertical welded bar segment. Furthermore, the formation of the fictitious hinge and then the rotation about it is combatted by the additional tension force provided by the NSM steel bars. Results indicate that the horizontal cracks at the compression face occurred within a thin concrete layer. At a load of 400 kN, bond failure occurred, resulting in a rapid extension of cracks followed by a diagonal path to join the horizontal crack developed at the compression face. The full collapse occurred at a load level of 425kN.

Regarding the beam portion, more cracks developed close to the anchorage of the main steel of the beam (nodal point CTT) relative to specimen C001 and RN01, referring to the high strength developed within the half-joint region. No cracks extended above the embedded horizontal bars. It is expected that if the bond failure is avoided by using suitable anchors or welding the bars to plate fixed on the face of nib end, higher capacity may be obtained.

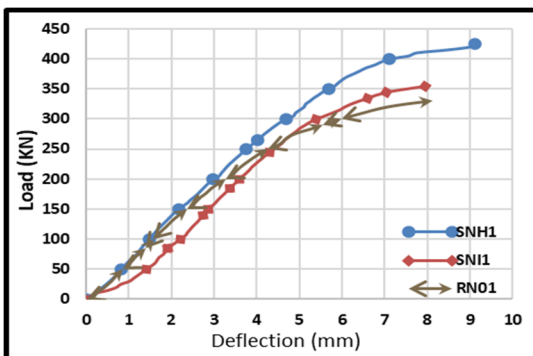
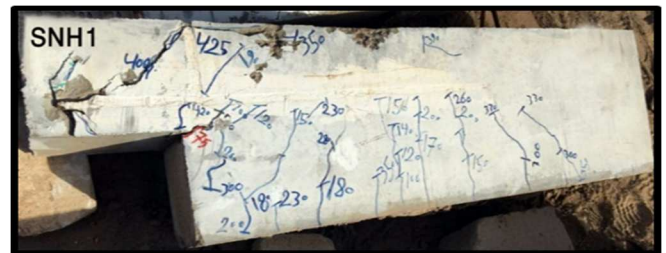
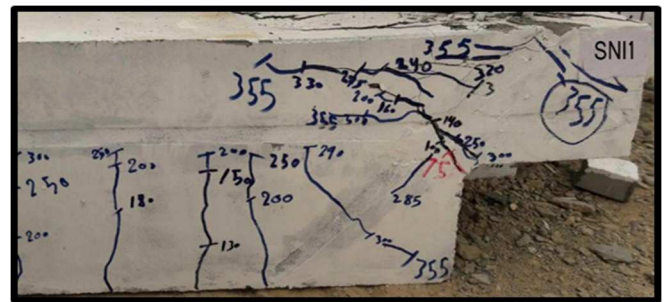


Fig. 9 Effect of strengthening nib region on the response (a/d=1.0)

The configuration SN11, Fig. 10b, shows that the first crack initiated at the re-entrant corner with an angle of about 45°. Beyond the strengthening bars, the crack extended with a smaller angle of less than 30°. In this scheme, the bond failure of the specimen SNH1 is avoided by extending the horizontal bars to the tip of the nib end and using the diagonal welded bars. An additional tie force across the diagonal crack at which the fictitious hinge lies is provided to resist the two parts' free rotation for the hinge. The beam portion responds more rigid, cracking concentrated close to the anchorage of the main steel, and no crack penetrated across the horizontal bars. Specimen failed when the compression resistance is violated due to concrete crushing of the compression zone.



(a) Specimen SNH1



(b) Specimen SN11

Fig. 10 Crack patterns for strengthening dapped ends SNH1 & SN11.

D. Specimen Control Reduced Reinforcement (RH01)

The load-deflection curve against specimen C001 is shown in Fig. 11. It can be noticed that the reduction in hanger reinforcement results in a slight decrease of the failure load by about 6%. This may be attributed to the fact that the concrete (high strength concrete) resists most of the shear stresses produced within the dapped end region. Then, the hanger's steel will be less effective than the case of dapped ends with normal strength concrete. Also, comparing the crack pattern for specimen RH01.

Fig. 12 shows the cracking pattern at failure. Results depicted that the first crack developed at 70 kN with a small angle (less than 20°). With progress in loading, the dapped end tends to deform as two parts rotating about the fictitious hinge due to the lack of force in the hanger tie, and noticeable curvature occurred for the beam portion resulting concrete crushing at the compression face and propagation of cracks is recognized near the anchorage end of the main tension steel. The failure occurred when the compression force is violated. Compared to specimen C001, few cracks developed within nib end due to its strength and the reduced force in the vertical tension tie. The failure of this specimen occurred by diagonal shear failure in the re-entrant corner.

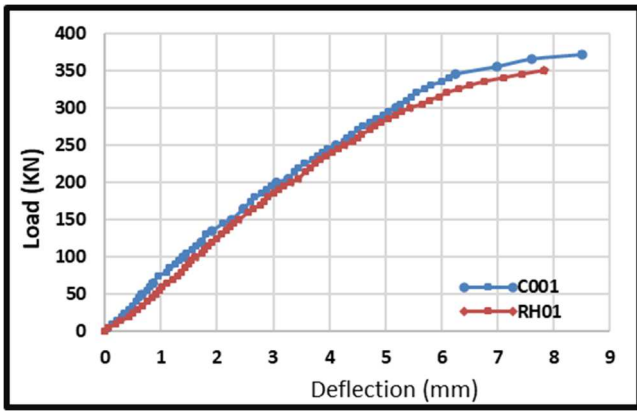


Fig. 11 Load-deflection curves of the specimen (RH01) against (C001)

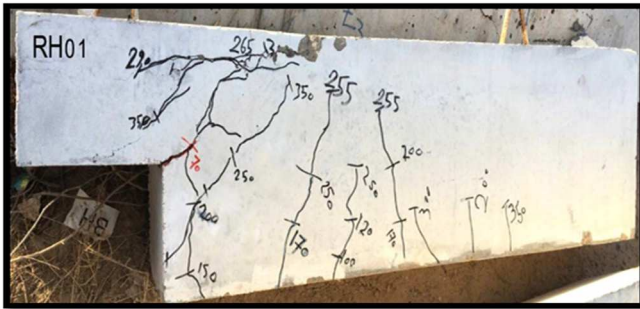


Fig. 12 Cracks patterns for the specimen with reduced reinforcement at the hanger

E. Specimens strengthened at the Hanger region (SHV1, SHT1 and SHF1)

Three configurations have been suggested to substitute the reduction of hanger reinforcement for $a/d=1.0$. The specimen (SHV1) is strengthened with two 2#10 vertical bars per side in hanger region while the other two specimens (SHT1) and (SHF1) are reinforced with 2#10 bars at angle 30° and 45° respectively at both sides in the hanger region. Fig. 13 shows the load deflection-curves that obtained for the three strengthened specimens against the specimen (RH01). The specimen (SHV1) yielded a stiffer response and load capacity (425kN) than the (SHF1) that yielded a load capacity (400kN), i.e., the increments in the failure load capacity were recorded by about (21%, 14.3%), respectively. However, specimen SHT1 yielded a small capacity (335kN), and a premature failure occurred. Fig (14 a, b, and c) show the three specimens' crack patterns, respectively. The vertical strengthening, Fig.14a, restricts the propagation of diagonal cracks, to some stage, close to the re-entrant corner at which the first crack occurred. The failure occurred due to the vertical cracking at the hanger zone that penetrates diagonally towards the load application. Therefore, it is expected the cracks may be further delayed by making some of the strengthened bars to be inclined or making the strengthening bars as in C shape.

Fig. 14b shows the crack pattern for the specimen SHT1. Adopting strengthening angle of 30°, a lack of reinforcement in the bottom corner of the full depth beam can be seen. Consequently, the small component of the axial force and that the provided bond length might be inadequate. Thus, the failure did not occur at the re-entrant corner. Then, it is expected that the capacity can be enhanced using a greater number of steel bars with smaller sizes within the disturbed regions of the beam.

Fig. 14c shows the map of crack propagation for the specimen SHF1, and failure occurred due to the lack of the anchoring force caused by the bond failure of the strengthening force bars at the bottom CTT nodal point. Thus, some curvature occurred, resulting in crushing at the compressive face. Failure of both SHT1 and SHF1 specimens happened at the full depth beam within the dapped end region and was caused due to bond failure.

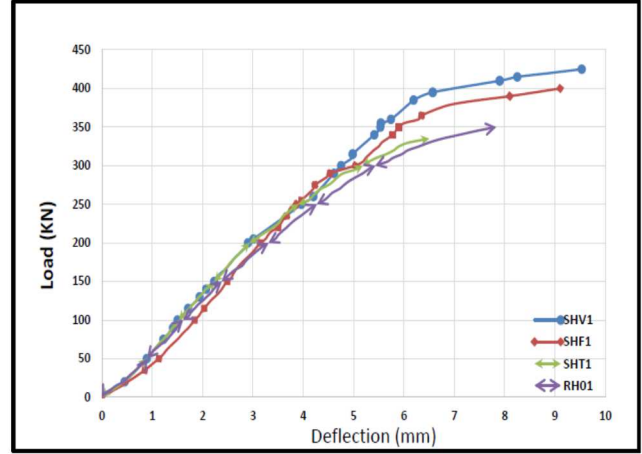
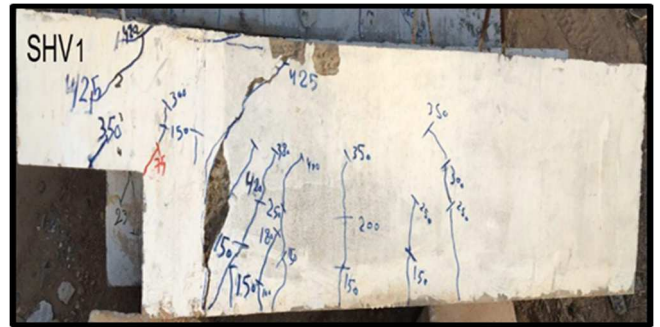


Fig. 13 Effect of strengthening configuration (at hanger region) against RH01.



(a) Specimen SHV1



(b) Specimen SHT1



(c) Specimen SHF1

Fig. 14 Crack pattern for the specimens (SHV1, SHT1 and SHF1)

F. Specimens SNH2 & SNI2; (a/d) = 1.5

The same detailing for specimens SNH1 and SNI1 is adopted for SNH2 and SNI2, but the tests are achieved under (a/d) value of 1.5. The testing goal is to check the influence of this variable on this technique's strengthening process and activity with a/d value larger than 1.0. Comparing the load-deflection curve of these specimens against the specimen (RN02) as shown in Fig. 15, the ultimate load capacity has improved by about (20% and 24%), respectively.

The crack pattern for the specimen SNH2 is shown in Fig. 16a. The first crack initiated at the re-entrant corner with a load of 50 kN and an angle of 60°. The addition of the horizontal NSM bars restricted the formation the fictitious hinge to some extent and the rigid body rotation of the two portions. It can be noticed that due to the existence of tension ties, the two parts acted as one unit within service loading. Thus, cracks propagated from the nodal point (CTT) and developed towards the zone of maximum moments. At load level of 250 kN, horizontal cracks propagated at the compression face. At load level of 285 kN, Bond failure occurred between the steel bars and epoxy. At this instant, the resistance to rotation about the fictitious hinge dropped leading to the formation of a new vertical crack at the re-entrant corner that penetrated rapidly caused a violation of equilibrium and causing a full collapse of the specimen.

Fig. 16b shows the map of cracking for the specimen SNI2. i.e. strengthening of the specimen RN02, by the mixed strengthening (horizontal and diagonal bars) scheme. It can be observed that the formation of the center of rotation that makes the nib and beam portion to rotate as rigid bodies is restricted and delayed up to the final stages of loading. The first crack developed from the re-entrant corner with an angle of about 40°. results depicted that the diagonal NSM bars restricted developing the cracks at the beam's bottom corner. With progress in loading, some curvature occurred, resulting in increasing the compressive stress up to the formation of horizontal cracks. At a load of 295 kN, bond failure occurred followed by rapid propagation of cracks within the extended end and around the re-entrant, leading to the specimen's full collapse.

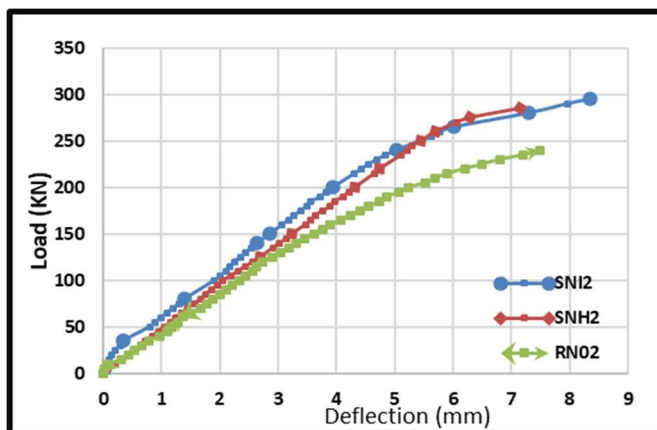
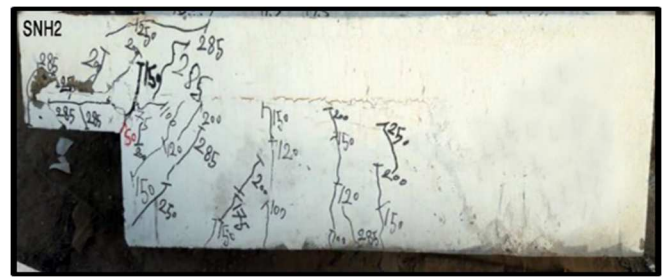
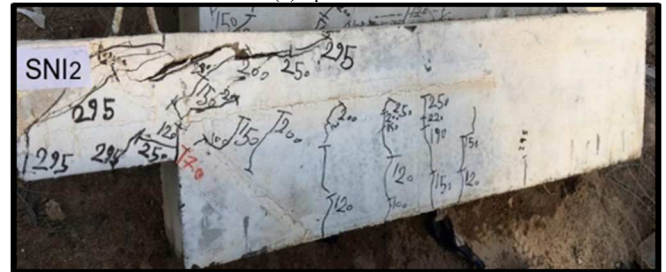


Fig. 15 Effect of strengthening configuration (at nib region) against RN02.



(a) Specimen SNH2



(b) Specimen SNI2

Fig. 16 Crack patterns for strengthening for specimens strengthened against main nib steel (a/d=1.0)

G. Toughness, Stiffness and Ductility

1) *Toughness Values:* Fig. 17 shows the calculated toughness values for the tested specimens. For a/d=1.0, reducing the nib steel by 50% resulted in diminishing the dissipated energy before failure (17%). Strengthening the deficient nib reinforced half-joints with horizontal bars led to enhanced toughness by (43%) relative to specimen RN01. Thus, it is recommended to adopt such strengthening configuration. However, the configuration SNI1 is not adequate because the force induced in the inclined bars is resolved into two-component. Then, reducing the horizontal component's value equilibrate the compressive strength above the NA (at the top of the beam).

The effect of reducing of hanger reinforcement on the dissipated energy may be understood by comparing toughness value for specimen RH01 with that for the control specimen C001, a reduction of (29%) has been obtained. For specimen SHV1, vertical bars are added for both sides at the hanger region to upgrade the weakness in the hanger stirrups' tension force. The toughness was enhanced by (87%) relative to the specimen RH01.

It is evident that the highest value of the dissipated energy with the strengthening configuration at which the strengthening bars are vertical such bars acted directly to resist tensile force. For the configuration of inclined embedded bars with 45° from horizontal, the enhancement in toughness relative to specimens C001 and RH01 are obtained to be (11%) and (57%).

Steel bars in the inclined configuration may act to reduce the penetration of the diagonal crack from the re-entrant corner or the bottom corner of the beam (CTT nodal point). For the configuration SHT1, the dissipated energy is small relative to the two other configurations and the control specimen C001; this may be due to the premature failure occurred. For the specimens with a/d=1.5, there is a significant drop in toughness relative to the corresponding specimens with a/d=1.0. For the reference specimen C002, the reduction is obtained to be 37%. For the reduced steel hanger specimen RN02, the reduction is observed to be 44%, while

for the strengthened specimen with horizontal bars (SNH2), the drop of toughness is 56%. Slight enhancement in performance is noticed for the specimen strengthened using the mixed configuration (SNI2) of (3%) relative to the specimen SNI1.

It can be concluded that the toughness is reduced when adopting large values of a/d ratios, because that the cracking propagation occurred and concentrated at the nib end which may be caused either to the small depth or deficient nib reinforced sections. Furthermore, the strengthening by horizontal configuration for the deficiently reinforced specimens yielded the best performance in terms of safety. At the same time, the vertical configuration yielded the best performance for the deficient reinforced hanger zone.

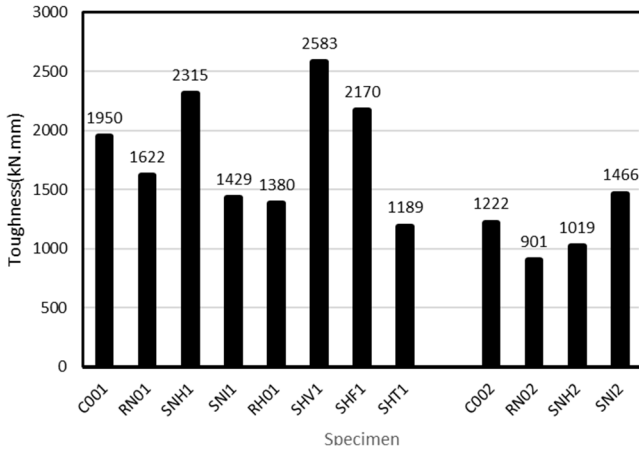


Fig. 17 Toughness values for the tested dapped ends

2) *Effective Stiffness*: According to Vu *et al.* [23], stiffness can be calculated from Equation 1 as follows:

$$K_e = P_1 / \Delta_1 \quad (1)$$

P_1 is $0.75 \times$ failure load, and Δ_1 is the corresponding displacement (18). Fig. 19 shows the effective stiffness of the tested half-joints. In general, results indicated that the stiffness reduced with increasing the a/d value. For the reference specimen (C002), the reduction is found to be 29% relative to specimen C001. Also, the a/d value has some effect on the stiffness of the deficiently reinforced sections at the extended end by 25% reduction relative to specimen RN01.

For the strengthened specimens SNH2, results indicate that the drop in stiffness is 33% close to the corresponding specimen SNH1. Whereas for the specimen SNI2, stiffness is reduced by 10% compared to specimen SNI1. Specimen SNH1 yielded higher stiffness than SNI1. This means that there is excellent resistance to deformation and cracking propagation by using the strengthening arrangement SNH1. However, with a higher a/d ratio, the configuration SNI2 seems to yield better resistance to deformations.

For the specimen RH01, it can be observed that there is no significant drop in stiffness due to a reduction in hanger reinforcement by 30%. This may be attributed to the fact that the role of hanger stirrups to interrupt the diagonal crack from the re-entrant corner is replaced partially by the concrete's high strength.

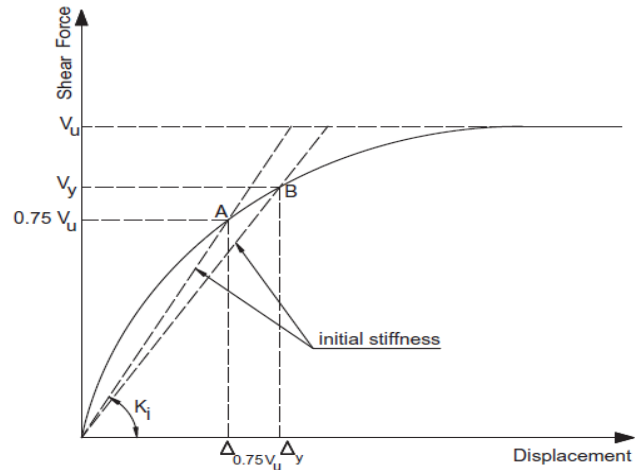


Fig. 18 Effective stiffness determination [23]

For the strengthened specimens at the hanger region, it can be observed that the useful stiffness for samples SHV1, SHF1 and SHT1 have the same stiffness as the reference specimen. It can be drawn out that providing enough embedded length of the strengthening bars for SHT1 may enhance the performance of the half-joint in terms of toughness and ultimate capacity.

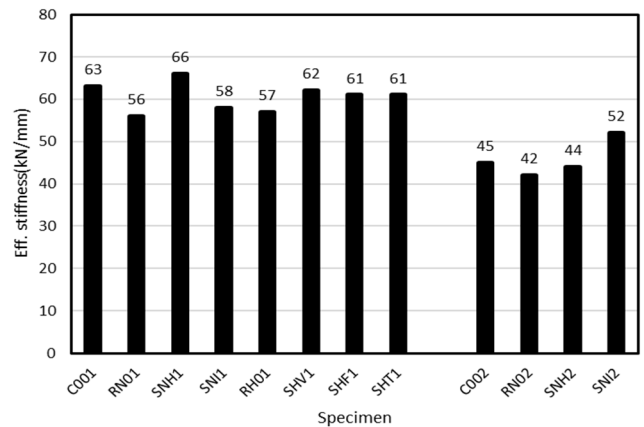


Fig. 19 Effective stiffness for the tested specimens

3) *Ductility Ratio*: Ductility represents the extent of deformations before failure that a member may yield beyond yielding. Then, it is an indicator of the margin of safety that a member may provide. Two methods have predicted the ductility ratio for the tested specimens, the first is based on the displacement ratio, and it may be defined as the ratio of maximum displacement to a certain displacement which can be determined by intersections of the two tangents to the initial and final points of the load-deflection curve as shown in Fig. 20. Thus, the ductility ratio can be expressed as:

$$D1 = \mu = \Delta_{max} / \Delta_y \quad (2)$$

The second method is based on the energy dissipation throughout the full history of loading and that within the elastic stage only, as shown in Fig. 21. Then, the ductility ratio can be expressed as:

$$D2 = \mu = 0.5((E_{tot}/E_{el}) + 1) \quad (3)$$

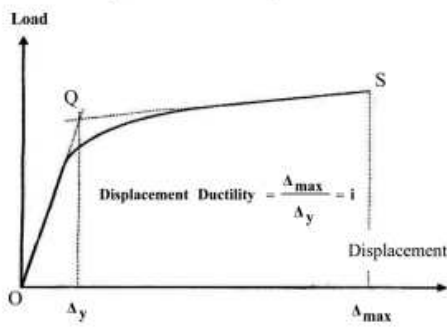


Fig. 20 Determination of ductility ratio by displacement method [24]

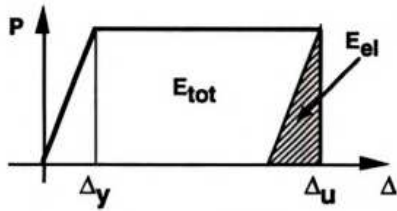


Fig. 21 Determination of ductility ratio by dissipated energy method [25]

In which E_t : is the total energy dissipated up to failure. E_e : is the energy that is proposed to be dispersed within the elastic stage (area of the hatched triangle). In which: E_{tot} is the total energy dissipated up to failure. E_{el} is predicted energy dissipated within the elastic stage of loading only. It can be seen from Equation 3 that the ductility value is affected only by the toughness ratios (total to the elastic). Sometimes this may not reflect the stage of failure, i.e., the difference in stages that specimens may fail, failure occurred due to exhausting capacity of materials or due to secondary reasons. It can be seen from Fig. 22 that for smaller a/d value, there is no significant difference in ductility values between the control, reduced, and strengthened specimens. However, for $a/d=1.5$, there is some sensitivity for the calculated concerning steel detailing. However, it is still less than the results of the method based on the displacement ratio. On the other hand, Equation 3 is affected directly by the stage of failure and stiffness at the initial and final stages. The reduction in values for specimens RN02, RNH2 and RNI2 relative to the specimen C002 are 11%, 16% and 4%, respectively. According to Equation 2, the corresponding values are 18%, 27%, and 12%. It can be concluded that the ductility calculated by Equation 3 is non-sensitive when there is a small difference in effective stiffness for the tested specimens, as shown in Fig. 19.

For $a/d=1.0$, reducing the nib and hanger steel reduced ductility by 12% and 13%, respectively. For the strengthened specimens SNH1 and SNI1, the reduction in ductility is found to be 13% and 26% relative to specimen C001, respectively. This number emphasizes the arrangement SNH1 yielded better results. For the strengthened specimens at the hanger region, the three configurations yielded the same reduction in ductility (15%) relative to the reference specimen C001.

For samples with $a/d=1.5$, the ductility ratio decreases relative to the corresponding specimens with $a/d=1.0$. For the control specimen C002, ductility was reduced by 7%. While for that with nib-reduced reinforcement, the reduction is noticed to be 13% compared to specimen RN01. Regarding

the strengthened specimen, SNH2, the drop in ductility is 22% relative to specimen RN01. However, slight enhancement in ductility is observed for specimen SNI2 compared to specimen SNI1 by 11%.

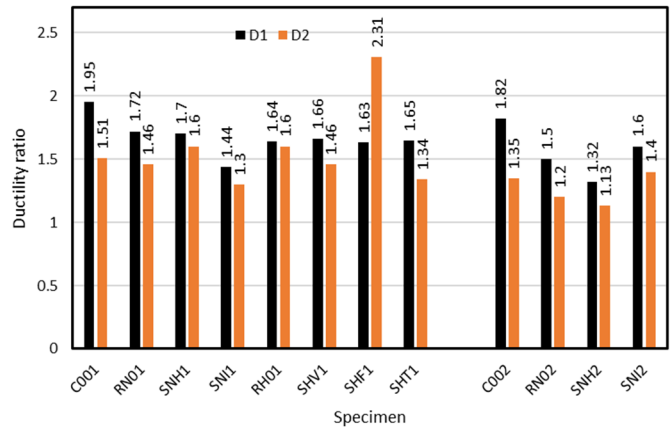


Fig. 22 Ductility ratios for the tested specimens based on displacement ratio (D1) and toughness ratio (D2)

IV. CONCLUSION

It found that (a/d) ratio has a noticeable effect on the behavior of dapped end beam. For the control specimens, the reduction of (a/d) ratio from (1.5) to (1.0), led to increasing the failure load capacity by about (32.6%) and shifting the mode of failure from diagonal tension in the extended end to diagonal shear failure at the re-entrant corner accompanied with crushing in the compression zone. Also, it is observed that the reduction of nib reinforcement by about (50%) has no essential effect on failure load, i.e., reduction of almost (5%) for $a/d=1.5$ and (11%) for $a/d=1.0$. Also, the decrease in hanger reinforcements by about (30%) reduced the failure load by about (6%) in the (a/d) ratio (1.0). This may be because the PCI method yields some overestimation when designing the self-compacting high-strength concrete.

The strengthening results found that strengthening the nib region with horizontal NSM steel bars led to increasing the failure load capacity by (29%) with $(a/d)=1$. While the enhancement in strength for a specimen with $(a/d)=1.5$ was about (20%). The increase in the strength capacity for strengthened hanger regions vertical and inclined bars for a/d (1) was about (21% and 14.3%) respectively.

For $a/d=1.0$, it is concluded that reducing nib steel by 50% resulted in reducing toughness by 17% whereas reducing the hanger steel by 30% led to a drop in toughness by 29%. For $a/d=1.5$, the reduction in toughness due to deficiently reinforced nib end resulted in a drop in toughness by 44%. Furthermore, it is found that strengthening of deficiently nib and hanger reinforced specimens with $a/d=1.0$, led to an improvement in toughness by 43% and 47%, respectively. For $a/d=1.5$, the strengthening for nib end deficiency led to a maximum enhancement in toughness by 62%.

It is concluded that the effective stiffness value is reduced by 29% when the a/d ratio increased from 1.0 to 1.5. Moreover, strengthening of deficiently reinforced nib end with $a/d=1.0$ resulted in improving stiffness by 18% whereas when, strengthening the hanger zone, the enhancement is 9%. For specimens strengthened at nib region and $a/d=1.5$, the enhancement in stiffness is 24%.

Regarding ductility, it is concluded that the ductility ratio prediction using the toughness ratio method may not express the behavior of the specimen. Whereas for the displacement ratio method, the failure stage is considered. Thus, it takes into consideration the cases of secondary types of failure that may result in deterioration of strength in relatively initial stages of loading.

REFERENCES

- [1] Precast Prestressed Concrete Institute. (2010). PCI Design Handbook: Precast and Prestressed Concrete 7th Ed.,2010. Chicago, IL.
- [2] Atta A. and Taman M., Innovative method for strengthening dapped-end beams using an external prestressing technique. *Materials and Structures*, 2016 49:3005–3019. DOI 10.1617/s11527-015-0701-8.
- [3] Mattock, A. H., and Chan, T. C., "Design and Behavior of dapped End Beams", *PCI Journal*, November-December, V.24, No. 6, pp. 28-45, 1979.
- [4] S. K. Liem, Maximum Shear Strength of Dapped-end or Corbel. MSc Thesis, College of Engineering, University Concordia, Montreal, Quebec, Canada, August 1983.
- [5] Lu W., Lin I., Hwang S. and Lin Y., "Shear strength of high strength concrete dapped-end Beams", *Journal of the Chinese Institute of Engineers*, Vol. 26, No. 5, pp. 671-680, 2003,
- [6] Ahmad S., Elahi A., Hafeez J., Fawad M. and Ahsan Z., "Evaluation of the Shear Strength of Dapped Ended Beam", *Life Science Journal*, V. 10, No. 3, pp. 1038-1044, 2013.
- [7] Aswin M., Mohammed B. S., Liew M. S., and Syed Z. I., "Shear Failure of RC Dapped-End Beams", *Hindawi Publishing Corporation Advances in Materials Science and Engineering*, 2015.
- [8] Tan K. H., "Shear Strengthening of Dapped Beams Using FRP Systems". *FRPRCS-5: Vol. 1: Proceedings of the fifth international conference on Fibre-reinforced plastics for reinforced concrete structures*, Cambridge, UK, 16–18 July 2001.
- [9] Nanni A. and Huang P. C., "Validation of an Alternative Reinforcing Detail for the Dapped Ends of Prestressed Double Tees" *University of Missouri-Rolla 224 Engineering Research Laboratory, PCI journal*, 2002.
- [10] Afefy, H. M. E., Mahmoud, M. H., Fawzy T. M., "Rehabilitation of defected RC stepped beams using CFRP"; *Engineering Structures*, Vol. 49, pp. 295–305, 2013.
- [11] Sas G., Dăescu C., Popescu C., Nagy-György T., "Numerical optimization of strengthening disturbed regions of dapped-end beams using NSM and EBR CFRP". *Composites: Part B*, 2014.
- [12] Taher S. F., "External Strengthening of Critically Designed RC Girders with Highly Stressed Dapped-Ends" *Structural Engineering Department, Faculty of Engineering, Tanta University. Structures & Buildings*, 24 March, 2015.
- [13] Qasim M. Shakir, Baneen B. Abd "Strengthening of Self Compacting Reinforced Concrete Dapped End Beams with CFRP Sheets", *Journal of materials and Engineering Structures*, Vol. 6, 359–374, 2019.
- [14] Al-Mahmoud F., Castel A., François R., Tourneur C., "RC beams strengthened with NSM CFRP rods and modeling of peeling-off failure", *Composite Structures*, Vol. 92, pp 1920–1930, 2010.
- [15] Sabau C., Popescu C., Sas G., Schmidt J. W., Blanksvärd T., Täljsten B., "Strengthening of RC beams using bottom and side NSM reinforcement", *Composites Part B*, Vol. 149, pp 82–91, 2018.
- [16] Carrillo de Albornoz V.A., García del Toro E. M., Más-López M. I. and Patiño A. L., "Experimental Study of a New Strengthening Technique of RC Beams Using Prestressed NSM CFRP Bars", *Sustainability*, Vol.11, No. 1374; doi:10.3390/su11051374, 2019.
- [17] Yang Y., Fahmy M. F.M., Cui J., Pan Z., Shi J., "Nonlinear behavior analysis of flexural strengthening of RC beams with NSM FRP laminates", *Structures*, Vol. 20, 374–384, 2019.
- [18] Al Rjoub Y. S., Ashteyat A.M., Obaidat Y. T. & Bani-Youniss S., "Shear strengthening of RC beams using near-surface mounted carbon fibre-reinforced polymers", *Australian Journal of Structural Engineering*, Vol. 20, issue 1, 2019.
- [19] Yu X., Xing G., Chang Z., "Flexural behavior of reinforced concrete beams strengthened with near - surface mounted 7075 aluminum alloy bars", *Journal of Building Engineering*, Vol. 31 101393, 2020.
- [20] Askandar N. and Mahmood A., "Comparative Investigation on Torsional Behaviour of RC Beam Strengthened with CFRP Fabric Wrapping and Near-Surface Mounted (NSM) Steel Bar", *Advances in Civil Engineering*, Vol. 2019, <https://doi.org/10.1155/2019/9061703>.
- [21] Qasim M. Shakir, Hayder H. H. Kamonna., "The Behavior of High Strength Self-Compacting Reinforced Concrete Corbels Strengthened with NSM Steel Bars". *International journal on Advanced Science Engineering Information Technology* Vol. 8, No. 4, 2018.
- [22] Wang Q., Guo Z., Hoogenboom, P. CJ, "Experimental investigation on the shear capacity of RC dapped end beams and design recommendations", *Structural Engineering and Mechanics*, Vol. 21, No. 2, pp 221-235, 2005.
- [23] Vu N. S., Bing L., Beyer K., "Effective stiffness of reinforced concrete coupling beams", *Engineering Structures*, Vol. 76, pp 371–382, 2014.
- [24] Rakhshanimehr M., Esfahani M. R., Kianoush M. R., Mohammadzadeh B. A., and Mousavi S. R., "Flexural ductility of reinforced concrete beams with lap-spliced bars", *Can. J. Civ. Eng.*, Vol. 41, No. 7, pp 594–604, 2014.
- [25] Naaman A. and Jeong S., "Structural ductility of concrete beams prestressed with FRP tendons", In: *Proc. Second Int. RILEM Symp. (FRPRCS- 2) Non-Metallic Concr. Struct.*, Ghent, Belgium, pp 379–86, 1995.